ioral data. The little brown bat (*Myotes lucifugus*) begins the approach phase for wire obstacles 0.3 cm in diameter at an average distance of 225 cm (*11*), and the horseshoe bat (*Rhinolophus ferrumequinum*) compensates for Doppler-shifted echoes only when delayed less than an average of 17.5 msec (301 cm) (*12*). The finding that bats react when targets are closer than 301 cm corresponds to our finding that the range axis ends at about 310 cm. *Eptescius fuscus, Phyllostomus hastatus, Pteronotus suapurensis*, and *R. ferrumequinum* are all able to discriminate range differences of 1.2 to 2.5 cm at an absolute distance of 30 to 60 cm (*13*). This also corresponds to our finding if we assume that the rate of change in best range (1.99 cm per neuron) is the theoretical limit of just-noticeable difference in distance.

Delay-tuning curves themselves are sometimes insufficient to express the properties of range-tuned neurons and may even be misleading. Their responses are more appropriately expressed by iso-impulse-count contours plotted on coordinates of echo amplitude against delay. In Fig. 2, for instance, the neuron is clearly tuned to an echo of 37 dB SPL delayed by 2.1 msec. Range information is apparently processed by a series of such neural filters in both the time and amplitude domains, and as such they may be considered cross-correlators (*14*).

Odotopic representation is the term we use to describe the representation of target range by the location of neurons tuned to different BD's. This representation is the same regardless of wide variations in repetition rate (10 to 100 per second) and signal duration (7 to 34 msec). In the auditory system, the synthesis of a range axis, which has no corresponding anatomical precursor in the periphery, is suggestive of the methods by which sensory information may be extracted and displayed in the brain.

When many conspecific bats echolocate in a confined space, their many orientation sounds and echoes would impair odotopic representation unless some mechanism protected the system from jamming. The fundamental harmonic (H_1, particularly FM_1) of the orientation sound is always critical to the response of range-tuned neurons in spite of the fact that H_1 is always much weaker than the other harmonics and is sometimes barely detectable in laboratory recordings. This means that range-tuned neurons are probably not excited by combinations of orientation sounds and echoes produced by bats flying nearby. To excite range-tuned neurons, H_1 must stimulate the ears prior to an echo in spite of its weakness in the emitted sound. This implies that H_1 produced by the vocal cords stimulates the animal's own ears by bone conduction but is not emitted at a significant amplitude, possibly because of suppression by vocal-tract antiresonance. In nature, range-tuned neurons would be selectively excited only when the animal itself emits orientation sounds and echoes return after particular short delays. Jamming is thereby avoided in most situations.

NOBUO SUGA, WILLIAM E. O'NEILL
Department of Biology, Washington University, St. Louis, Missouri 63130

References and Notes

1. N. Suga, *Fed. Proc. Fed. Am. Soc. Exp. Biol.* **37**, 2342 (1978); _____ and P. H.-S. Jen, *Science* **194**, 542 (1976).
2. N. Suga, *Science* **196**, 64 (1977).
3. T. Manabe, N. Suga, J. Ostwald, *ibid.* **200**, 339 (1978).
4. N. Suga, W. E. O'Neill, T. Manabe, *ibid.*, p. 778.
5. W. E. O'Neill and N. Suga, *ibid.* **203**, 69 (1979).
6. N. Suga, W. E. O'Neill, T. Manabe, *ibid.*, p. 270.
7. A. Novick and J. R. Vaisnys, *Biol. Bull. (Woods Hole)* **127**, 478 (1964).
8. The best delay is the echo delay at which the minimum threshold for facilitation is obtained. Best delay corresponds to the best range of a neuron.
9. For mimicking orientation sounds and echoes (inset, Fig. 1C) (*4, 5*) in the three phases of echolocation, the repetition rate of paired stimuli and the durations of the CF and FM components of the signal were, respectively, 10 per second, 30 msec, and 4 msec (search phase); 40 per second, 15 msec, and 3 msec (approach phase); and 100 per second, 5 msec, and 2 msec (terminal phase). Synthesized echoes were independently varied in frequency, amplitude, and delay from the synthesized orientation sounds. To identify which combination of signal components was essential for excitation of neurons, both the synthesized orientation sounds and echoes were independently simplified by eliminating individual signal components.
10. The sulcus cannot be used as an anatomical reference line since iso-BD contour lines are neither straight nor parallel to it. In each oblique electrode penetration, BD's between 4 and 6 msec were recorded. Therefore, the data for each entire penetration were shifted to be in register with those values. The relative distances between individual data points within each penetration are not affected by this technique.
11. A. D. Grinnell and D. R. Griffin, *Biol. Bull. Woods Hole* **114**, 10 (1958).
12. G. Schuller, *Naturwissenschaften* **61**, 171 (1974).
13. J. A. Simmons, *Ann. N.Y. Acad. Sci.* **188**, 161 (1971); _____, D. J. Howell, N. Suga, *Am. Sci.* **63**, 204 (1975).
14. N. Suga, *Shizen* **79-6**, 70 (1979).
15. We thank J. Jaeger for his assistance in our auditory laboratory and E. G. Jones for kindly providing frozen sections of the brain of the mustache bat. Supported by NSF grant BNS 78-12987 to N.S. and by PHS training grant 1-T32-NS07057-01 to W.E.O.

30 March 1979; revised 2 July 1979

Laser-EXAFS: Fast Extended X-ray Absorption Fine Structure Spectroscopy with a Single Pulse of Laser-Produced X-rays

Abstract. *The extended x-ray absorption fine structure (EXAFS) spectrum of aluminum has been measured with a nanosecond pulse of soft x-rays generated by a laser-produced plasma. This technique provides a practical alternative to synchrotron radiation for the acquisition of EXAFS data. It also provides a unique capability for the analysis of molecular structure in highly transient chemical species.*

Determining the identities and exact spatial arrangement of the atoms surrounding any particular atom in a molecule is fundamental to understanding the properties of any type of liquid, gas, or solid. In the case of materials with long-range order, such as perfect crystals, this information can often be obtained with x-ray or particle beam diffraction techniques. Such diffraction techniques rely on the fact that all of the atoms in a perfect lattice reside at fixed, periodic distances from any given atom, and that this periodicity is retained regardless of how far one moves within the lattice from the atom in question.

For materials without long-range order, the diffraction techniques are far less useful; one can determine local configurations in this way only for relatively simple molecules composed of a single element. For more complicated molecules, considerable insight can often be gained from optical spectroscopy and magnetic resonance techniques. However, these techniques have the drawback of providing only indirect evidence, from which the structural parameters of interest for a molecule must be inferred.

Many of these limitations can be overcome with the recently developed technique of extended x-ray absorption fine structure (EXAFS) spectroscopy (*1, 2*). In EXAFS spectroscopy, the x-ray absorption coefficient of a material is measured as a function of energy from the *K* edge or *L* edge of a specific element in the material to as far as 1000 eV above the edge. The absorption of x-rays by the element is accompanied by the ejection of photoelectrons, which can be scattered from neighboring atoms. Backscattering of these photoelectrons from atoms in the immediate vicinity of the absorbing atom gives rise to a periodic "wiggle" structure in the x-ray absorption spectrum (*1, 3, 4*). By analyzing this wiggle structure above the absorption

0036-8075/79/1019-0353$00.50/0

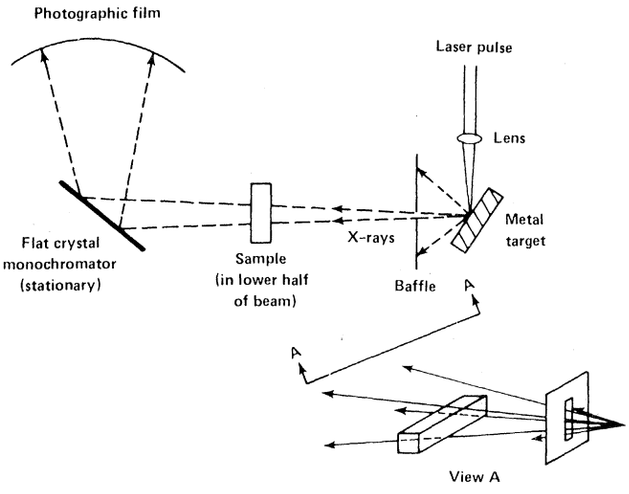

Fig. 1. Schematic top view of laser-EXAFS experimental configuration showing (*View A*) the positioning of the sample in the x-ray beam.

edge of a particular element, information can be obtained about the spatial arrangement of atoms in the immediate vicinity of the absorbing species. Since only the nearby atoms are involved, long-range order is not required; therefore, the EXAFS technique can be applied to the study of a broad class of materials, including liquids, gases, and amorphous or crystalline solids.

In the past, chemical structure research with the EXAFS technique has been limited by the lack of suitably intense sources of x-rays. This deficiency is now being remedied to some extent by the increasing availability of synchrotron radiation, which is being harnessed in a number of x-ray test facilities throughout the world (*5*). Certain types of EXAFS experiments, however, cannot be performed easily with synchrotron x-ray sources. Most significant, perhaps, are experiments designed to analyze highly transient structures such as chemically reactive intermediates or the excited electronic states of molecules. These experiments could be carried out if it were possible to obtain a complete EXAFS spectrum with a single, intense, short pulse of x-rays synchronized with the optical or electrical excitation of the sample. Previous work in our laboratories has indicated that laser-produced plasmas should be nearly ideal x-ray sources for experiments of this type (*6*).

We report here that it is possible to obtain well-resolved EXAFS spectra of light elements (atomic numbers up to about 40) with a single pulse of soft x-rays produced with a neodymium-doped-glass laser. The basic experimental configuration is shown in Fig. 1. In a typical experiment, an infrared laser pulse with an energy of approximately 100 J and a pulse width of approximately $3^1/_2$ nsec (full width at half-maximum) is focused onto a solid metal slab target, thereby creating a surface plasma and raising it to the kilovolt temperature regime by means of the inverse bremsstrahlung absorption process. The laser pulse strikes a focal spot 100 to 200 μm in diameter at an incident intensity of about 10^{14} W/cm^2. The resulting x-ray spectrum is dispersed by Bragg reflection from a flat KAP (potassium acid phthalate) crystal and recorded on photographic film. The position and range of the recorded spectrum can be varied easily by adjusting the size and position of the dispersing crystal. As shown in Fig. 1, the system is so arranged that the thin-film sample occupies half of the x-ray beam. The reflected (diffracted) x-rays thus form a double image on the photographic film, with the reference portion of the reflected beam striking the top half and the sample portion of the beam striking the lower half of the film. In this way, the entire spectrum is recorded at once, using a single laser pulse. The EXAFS spectrum can easily be extracted from the data since the incident and transmitted x-ray intensities are known for each wavelength.

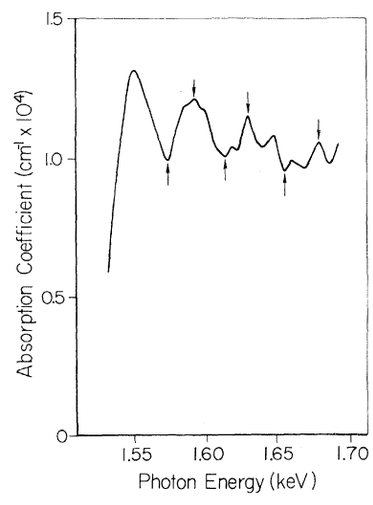

Fig. 2. Laser-EXAFS spectrum of aluminum foil.

We used film because the need to record the entire spectrum in a few nanoseconds rules out detectors based on the counting of individual photons. Film is the simplest alternative and, when evaluated by digital densitometer techniques, is capable of high resolution and contrast discrimination. With proper choice of film type, grain size, exposure, and data handling, it is possible to obtain results approaching the statistical limit allowed by the incident x-ray photon fluence. Because the photographic film is a nonlinear recording medium, it is necessary to multiply the measured optical densities by a known response factor to determine the absolute x-ray flux at each wavelength. This data handling is done with an on-line minicomputer.

The capabilities of this technique are illustrated by the laser-EXAFS spectrum, shown in Fig. 2, of a thin (2.0 μm) foil of aluminum (*7*). This spectrum is representative of our results to date and was obtained with the x-rays produced by a single laser pulse incident on an iron slab target. Iron was chosen as the target material because it produced mainly continuum emission in the vicinity of the aluminum *K* edge. The same EXAFS spectrum was obtained when the sample was exposed to a pulse of x-rays produced by a copper laser target, showing that the results obtained by this technique are independent of the target material, at least for targets with relatively smooth x-ray emission in the vicinity of the absorption edge being studied.

The measured spectrum can be interpreted on the basis of the generally accepted formula for EXAFS (*1*)

$$\chi(k) = \frac{m}{4\pi\hbar^2 k} \sum_j \frac{N_j}{R_j^2} t_j(2k) \exp\left(\frac{-2R_j}{l}\right) \times \sin[2kR_j + 2\delta_j(k)] \exp(-2k^2\sigma_j^2) \quad (1)$$

Here $\chi(k)$ is the fractional modulation of the absorption coefficient due to EXAFS: $\chi(k) = (\mu - \mu_0)/\mu_0$, where μ_0 is the absorption coefficient for a single atom in a vacuum. The quantity $k = [0.262467(E - E_{edge})]^{1/2}$ is the photoelectron wave vector in reciprocal angstroms, where E is energy in electron volts; m is the electron mass; h is Planck's constant; N_j is the number of atoms scattering at the distance R_j; $t_j(2k)$ is the electron scattering matrix in the backward direction for atoms at R_j; l is the mean free path of the electron; $\exp(-2\sigma_j^2k^2)$ is a Debye-Waller factor due to thermal vibrations or static disorder with root-mean-square fluctuations σ_j; and $\sin[2kR_j + 2\delta_j(k)]$ is the si-

nusoidal interference term, $\delta_j(k)$ being the phase shift. A full analysis of the spectrum on the basis of Eq. 1 requires the use of computer-assisted Fourier transform techniques (*1*, *2*). However, it is more illustrative for the present purpose to employ a straightforward graphical technique (*1*) to deduce the nearest-neighbor distance.

The graphical technique is based on the fact that the EXAFS curve is usually dominated by scattering from the nearest neighbor. This is especially true of the positions of the principal maxima and minima, which are determined mainly by the first sine term in Eq. 1, namely $\sin[2kR_1 + 2\delta_1(k)]$. If δ_1 is linear in k, then $\delta_1 = \alpha_1 k + \beta_1$, and the argument of the sine term takes the form $2k(R_1 - \alpha_1) + 2\beta_1$. The approximate positions of the maxima and the minima of the EXAFS curve are thus given by

$$n\pi = 2k(R_1 - \alpha_1) + 2\beta_1 \qquad (2)$$

where $n = 0, 2, 4, \ldots$ for maxima and 1, 3, 5, . . . for minima. A plot of n against k for the dominant maxima and minima of the EXAFS spectrum shown in Fig. 2 is given in Fig. 3 with $k = 0$ taken to correspond to the inflection point, $E_{K\,\mathrm{edge}} = 1552$ eV, of the measured x-ray absorption coefficient. The points closely fit a straight line with a slope $(2/\pi)(R_1 - \alpha_1)$ of 1.7 Å. This leads to the basic result $(R_1 - \alpha_1) \approx 2.6$Å. Since $R_1 >> \alpha_1$ (α_1 is typically a few tenths of an angstrom), this result is in good agreement with the known nearest-neighbor distance of 2.86 Å for the aluminum face-centered-cubic lattice (*8*).

The spectrum presented in Fig. 2 is noteworthy for several reasons. It illustrates the capability of the laser-EXAFS technique to record EXAFS spectra of light elements with absorption edges below about 3 keV, which are difficult to study with other x-ray sources. The technique is particularly suitable at present for the study of *K*-edge EXAFS spectra of the elements from carbon to sulfur and of *L*-edge EXAFS spectra of the elements from sulfur to molybdenum. More important, however, the complete laser-EXAFS spectrum presented in Fig. 2 was obtained in only a few nanoseconds with a single pulse of laser-produced x-rays. This represents a dramatic improvement in the speed and ease of obtaining EXAFS data compared to what is possible with other known x-ray sources. The technique also makes possible the measurement of "flash-EXAFS" spectra of transient species having lifetimes of a few nanoseconds or less. Thus, with this technique it may soon be possible to make "snapshots"

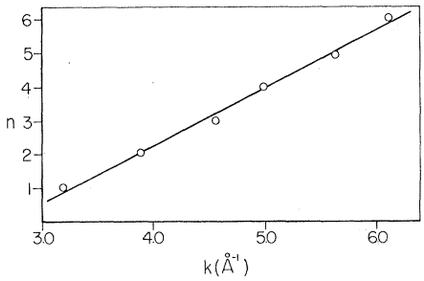

Fig. 3. Graph of n versus k for aluminum. The points correspond to the features indicated by arrows in Fig. 2.

or "movies" of the structural changes that occur in molecules when they are excited by optical or other means. If this proves to be the case, laser-EXAFS will have provided an important new dimension to the study of chemical structure by x-ray absorption techniques.

P. J. MALLOZZI, R. E. SCHWERZEL
H. M. EPSTEIN, B. E. CAMPBELL
Battelle, Columbus Laboratories, Columbus, Ohio 43201

References and Notes

1. D. E. Sayers, F. W. Lytle, E. A. Stern, *Adv. X-Ray Anal.* **13**, 248 (1970); F. W. Lytle, D. E. Sayers, E. A. Stern, *Phys. Rev. B* **11**, 4825 (1975); E. A. Stern, D. E. Sayers, F. W. Lytle, *ibid.*, p. 4836.
2. P. Eisenberger and B. M. Kincaid, *Science* **200**, 1441 (1978); S. P. Cramer, T. K. Eccles, F. Kutzler, K. O. Hodgson, S. Doniach, *J. Am. Chem. Soc.* **95**, 8059 (1976); S. P. Cramer and K. O. Hodgson, *Prog. Inorg. Chem.* **25**, 1 (1979).
3. R. de L. Kronig, *Z. Phys.* **70**, 317 (1931); *ibid.* **75**, 191 (1932); *ibid.*, p. 468; H. Peterson, *ibid.* **98**, 569 (1936).
4. C. A. Ashley and S. Doniach, *Phys. Rev. B* **11**, 1279 (1975); P. A. Lee and J. B. Pendry, *ibid.*, p. 2795.
5. A. L. Robinson, *Science* **190**, 1074 (19 → W. D. Metz and A. L. Robinson, *ibid.*, p. 1186; H. Winick and A. Brenenstock, *Annu. Rev. Nucl. Part. Sci.* **28**, 33 (1978).
6. P. J. Mallozzi, H. M. Epstein, R. G. Jung, D. C. Applebaum, B. P. Fairand, W. J. Gallagher, in *Fundamental and Applied Laser Physics: Esfahan Symposium*, M. S. Feld, A. Javan, N. A. Kurnit, Eds. (Wiley-Interscience, New York, 1973), pp. 165–220; P. J. Mallozzi, H. M. Epstein, R. E. Schwerzel, *Adv. X-Ray Anal.* **22**, 267 (1978).
7. The aluminum foil was purchased from Reactor Experiments, Inc.
8. L. Pauling, *The Nature of the Chemical Bond* (Cornell Univ. Press, Ithaca, N.Y., ed. 3, 1960), chap. 11.
9. We thank K. O. Hodgson and E. A. Stern for encouragement and many helpful suggestions. Supported by Air Force Office of Scientific Research grant AFOSR-78-3575.

25 June 1979; revised 27 August 1979

Juvenile Hormone: Evidence of Its Role in the Reproduction of Ticks

Abstract. *Ovarian development, vitellogenesis, and embryogenesis in recently mated fed females of the soft tick* Ornithodoros parkeri *Cooley were prevented by topical application of the insect antiallatotropin precocene 2. The blockage was relieved by topical application of juvenile hormone. Cancellation of the anti-juvenile hormone effects of precocene 2 and the reestablishment of oogenesis (and oviposition in one specimen) by a naturally occurring insect juvenile hormone argues strongly for a physiological role of juvenile hormone in acarine reproduction.*

In this study we demonstrate that application of the antiallatotropic compound precocene 2 prevents oocyte development in the soft tick (Argasidae) *Ornithodoros parkeri* and that exogenous juvenile hormone III (JH III) repairs the blockage. Precocene 2 has been shown to cause precocious metamorphosis, prevent ovarian development, and induce diapause in various insects presumably by suppressing the function of the corpora allata (*1*). When applied to the tick *Argas persicus*, precocene is reported to induce sterility in adult females (*2*). However, it is not clear whether this effect results from a suppression of JH production. Indeed, precocene also blocks nymphal molting in these ticks, suggesting a more widespread disruption of normal development. Moreover, no convincing evidence of JH activity in ticks has yet been reported. We sought to determine (i) whether the effects of precocene on oocyte development in ticks are similar to those in some insects, and if so (ii) whether the effects are reversed by JH application.

Recently mated unfed female *O. parkeri* were allowed to feed to repletion on white laboratory mice 24 hours before we applied 0.5 mg of precocene in 2 μl of dimethyl sulfoxide (DMSO) to the dorsum of each tick (Table 1). Control ticks remained untreated or we applied 2 μl of DMSO. Seven days after the application of precocene, one group of ticks was given a second application of 0.5 mg of precocene in DMSO. All groups (ten ticks each) were maintained at 26°C and 85 percent relative humidity. Control ticks began oviposition on day 12 after feeding; they deposited an average of 316 eggs (untreated group) and 311 eggs (DMSO-treated group) per female with normal hatch beginning in both groups approximately 14 days after initiation of oviposition. Since no oviposition had occurred by day 56 after feeding in either of

0036-8075/79/1019-0355$00.50/0